Momentum distributions for (^{11}Li, ^{9}Li $+ n + n$) breakup reactions

H. Esbensen,[1,2] G. F. Bertsch,[1,3] and K. Ieki[1,*]

[1]Cyclotron Laboratory, Michigan State University, East Lansing, Michigan 48824
[2]Physics Division, Argonne National Laboratory, Argonne, Illinois 60439
[3]Institute of Nuclear Theory and Department of Physics, FM-15, University of Washington,
Seattle, Washington 98195

We have calculated the momentum distributions of the three fragments emitted in the breakup reaction (^{11}Li,^{9}Li $+ n + n$), induced by the Coulomb field from a heavy target, and made comparisons to recent three-body coincidence measurements. Our three-body model for ^{11}Li provides a good description of the measured relative momentum distribution for the two emitted neutrons, and also for the single-neutron momentum distribution. The predicted distribution for the ^{9}Li recoil is much narrower than observed; a plausible explanation is presented.

PACS number(s): 24.10.$-$i, 25.70.$-$z

I. INTRODUCTION

A large experimental and theoretical effort has been devoted to the study of the structure and breakup reactions of ^{11}Li. Some of the main objectives have been to measure the low-lying dipole-strength distribution and possible angular correlations between the two neutrons emitted in (^{11}Li, ^{9}Li $+ n + n$) reactions, induced by interactions with a heavy target. The first complete three-body coincidence measurements have now been performed [1–3]. The data form a very important supplement to previous measurements of (^{11}Li, ^{9}Li) reactions, which include cross sections [4], angular distributions of single neutrons [5,6], and the longitudinal and transverse momentum distributions of ^{9}Li fragments [7,8].

In this paper, we apply the three-body model for ^{11}Li that we had developed earlier [9,10]. Correlations between the two valence neutrons play a crucial role for the weak binding [9] (^{10}Li is unbound), and they enhance the dipole strength at very low excitations by almost 50% [10]. This enhancement has a very significant effect on the calculated (^{11}Li, ^{9}Li) cross section for a heavy target, since Coulomb dipole excitation is the dominant reaction mechanism. Thus, our model has been rather successful [11] in reproducing the fragmentation cross sections measured at 800 MeV/nucleon [8], where Coulomb dissociation is responsible for almost 60% of the cross section for a lead target. At intermediate energies, Coulomb dipole excitations are expected to be responsible for an even larger fraction of the cross section. This reaction mechanism also explains [12] the shape of the forward-angle, single-neutron angular distributions that have been measured by Anne et al. [5]. Moreover, the model has predicted quite accurately the width of the ^{9}Li longitudinal

momentum distribution measured by Orr et al. [7]. We shall therefore analyze the recent coincidence data obtained for a lead target by Sackett et al. [2] in terms of Coulomb dipole excitations followed by dissociation.

The recent data [1,2] show that the average velocity of ^{9}Li fragments is larger than that of the emitted neutrons. This has been ascribed to post Coulomb acceleration of the ^{9}Li fragment, when it is liberated in the vicinity of the target nucleus, and it has been interpreted in terms of a lifetime that is much smaller than what one would expect from the width of the low-lying dipole response of ^{11}Li [2]. In the calculations we present, we do not incorporate the effect of post-acceleration (or finite lifetime). We use first-order perturbation theory and assume, for simplicity, as we did in Ref. [10], that the incoming ^{11}Li nucleus follows a straight-line trajectory. We can therefore anticipate some discrepancy upon comparison to the measured recoil momentum distribution of the ^{9}Li fragments. The relative momentum distribution for the two emitted neutrons, on the other hand, is insensitive to the post-acceleration effect. We therefore expect that measurements of this distribution will provide a better test of our model.

We also make predictions for the energy dependence of the longitudinal momentum distribution for the ^{9}Li fragment and investigate possible signatures of an angular correlation between the two emitted neutrons.

II. BASIC FEATURES OF THREE-BODY MODELS

Let us first summarize some of the main features of our three-body model that are relevant to the calculation of momentum distributions. A simplifying approximation, which we had to make in order to use the two-particle Green's-function technique to calculate the ground state [9] and the dipole response [10] of ^{11}Li, was to ignore the kinetic-energy operator associated with the core motion. The excitation energy is therefore determined by the final-state momenta of the two neutrons in the rest frame of ^{11}Li as follows,

*On leave from Department of Physics, Rikkyo University, 3 Nishi-Ikebukuro, Toshima, Tokyo 171, Japan.

$$\Delta E = \frac{\hbar^2}{2m}(k_1^2 + k_2^2) + S_{2n} \ . \tag{1}$$

Our model predicts the two-neutron separation energy $S_{2n} = 0.2$ MeV. This is somewhat smaller than the recently measured value of 0.34 ± 0.05 MeV [13]. Let us also mention at this point that our neutron-core Hamiltonian was adjusted to produce a $p_{1/2}$ resonance at 0.8 MeV, which is somewhat larger than the value obtained in recent measurements [14,15], which is about 0.65 MeV.

In the following we consistently use the two-neutron separation energy that our model predicts. The ground-state rms distance between the two valence neutrons is 6.24 fm, and the rms distance between the core and the center of mass of the two valence neutrons is 4.93 fm. It is useful at this point to compare to the results obtained from Faddeev calculations [16,17], which are based on a stronger neutron-core interaction, with a $p_{1/2}$ resonance close to 0.5 MeV, and a more realistic finite-range neutron-neutron interaction. These calculations predict a two-neutron separation energy of 0.21 MeV and a rms distance of 6.32 fm between two neutrons, in good agreement with our results. The rms distance between the core and the two valence neutrons is 4.48 fm, which is smaller than our result—as one would expect for a stronger neutron-core interaction.

III. MOMENTUM DISTRIBUTIONS

We have previously studied the angular correlation of the two neutrons emitted in (^{11}Li, ^{9}Li) reactions [10]. One can express the cross section generated by Coulomb dipole excitations as a differential in the momenta of the two neutrons in the rest frame of ^{11}Li as follows,

$$\frac{d^6\sigma}{dk_1 dk_2} = g_L(\xi)\frac{d^6 B^L(E1)}{dk_1 dk_2} + g_T(\xi)\frac{d^6 B^T(E1)}{dk_1 dk_2} \ , \tag{2}$$

cf. Eq. (5.12) of Ref. [10]. This cross section has two components, a longitudinal (L) one and a transverse (T) one, which are generated by the Coulomb force from the target nucleus, acting along the beam direction and perpendicular to the beam direction, respectively. The magnitudes of the two components are determined by the functions

$$g_L(\xi) = \left[\frac{4\pi Z_T e}{3\hbar v}\right]^2 \xi^2 [K_1^2(\xi) - K_0^2(\xi)][1 - (v/c)^2] \ ,$$

$$\tag{3a}$$

$$g_T(\xi) = \left[\frac{4\pi Z_T e}{3\hbar v}\right]^2 \xi^2 \left[K_0^2(\xi) - K_1^2(\xi) + \frac{2}{\xi}K_0(\xi)K_1(\xi)\right] \ ,$$

$$\tag{3b}$$

where ξ is the adiabaticity parameter, which depends on the excitation energy ΔE, $\xi = R\,\Delta E/(\hbar\gamma v)$, and R is related to the distance of closest approach for which strong nuclear absorption sets in, Eq. (5.10) of Ref. [10].

We have introduced two dipole-strength distributions in Eq. (2), a longitudinal and a transverse component,

that depend on the directions of the two momenta. They are identical to the usual dipole-strength distribution when one integrates over all orientations. The longitudinal distribution is defined by

$$\frac{d^6 B^L(E1)}{dk_1 dk_2} = \frac{3}{k_1^2 k_2^2}\sum_{h_1,h_2}|f_{h_1 h_2}^{10}(k_1,k_2)|^2 \ , \tag{4}$$

where the sum is over the helicities of the two neutrons. The expression for the f amplitudes in terms of dipole matrix elements, phase shifts, and two-particle D-functions is given in Ref. [10]. The calculated dipole matrix elements include the effect of the neutron-core interaction as well as that of the neutron-neutron interaction in the final state. These final-state interactions have a dramatic effect on the dipole response. This is discussed in detail in Ref. [10].

We also illustrated in Ref. [10] the angular dependence of the distribution (4) for selected values of the energies of the two emitted neutrons. The distribution is invariant under rotations around the beam direction. The symmetry axis for the transverse component is perpendicular to the beam direction and falls in the scattering plane determined by the incident projectile and the target nucleus. Otherwise, the two distributions are identical, i.e., they are related by a simple rotation of 90°. We shall make use of this fact in the following.

A. Comparisons to three-body events

Let us first consider the spherical part of the momentum distributions associated with the ^{9}Li recoil and with the relative motion of the two neutrons. Using the fact that the transverse dipole-strength distribution can be obtained from the longitudinal dipole-strength distribution by a simple rotation of 90°, we obtain the following expression for the two momentum distributions,

$$\frac{d\sigma}{d|p_1 \pm p_2|} = \int dk_1 dk_2 [g_L(\xi) + g_T(\xi)]$$

$$\times \frac{d^6 B^L(E1)}{dk_1 dk_2}\delta(|p_1 \pm p_2| - |k_1 \pm k_2|) \ , \tag{5}$$

which is expressed in terms of the longitudinal dipole distribution. The numerical calculations were performed by accumulating and storing the dipole strength for fixed excitation energy and fixed $|p_1 \pm p_2|$. This makes it easy to repeat the calculation of the momentum distributions for different targets and beam energies. The calculation of the single-neutron momentum distribution is much simpler, since the angle integration over the orientations of the momenta of the two neutrons becomes trivial. Thus we obtain

$$\frac{d\sigma}{dp_n} = \int dk_1 dk_2 [g_L(\xi) + g_T(\xi)]\frac{d^2 B^L(E1)}{dk_1 dk_2}\delta(p_n - k_1) \ .$$

$$\tag{6}$$

When comparing our calculations to the data from Ref. [2], we shall also always include the detection efficiency. It has been parametrized as a simple function of the decay energy, Fig. 11 in Ref. [2], and it can therefore easily

be included in the calculations.

We show in Fig. 1 the two calculated distributions (5) and the single-neutron spectrum (6), together with the data [2] obtained at 28 MeV/nucleon on a lead target. The distributions have been normalized to 100, and the data points were normalized to minimize the χ^2. The two sets of neutron data are in good agreement with our calculations, whereas the measured recoil momentum distribution is shifted to higher momenta and has a significantly larger width. These discrepancies may be related to the post-acceleration effect mentioned earlier.

An interesting question is whether the angular correlation between the two neutrons has any effect on the distributions with respect to the two momenta, $|\mathbf{p}_1 \pm \mathbf{p}_2|$. The total spread of these two momenta are almost identical in our model (within 6–8 %, the spread of $\mathbf{p}_1 - \mathbf{p}_2$ being the larger), and the data suggest a similar result [2]. There is, however, a more significant effect at small momenta. In order to make it more visible, we show in Fig. 2 the spherical parts of the three-dimensional distributions,

$$\left[\frac{d^3\sigma}{d(\mathbf{p}_1 \pm \mathbf{p}_2)} \right]_{\text{sph}} = \frac{1}{4\pi|\mathbf{p}_1 \pm \mathbf{p}_2|^2} \frac{d\sigma}{d|\mathbf{p}_1 \pm \mathbf{p}_2|} \ , \qquad (7)$$

calculated without the efficiency correction. The two distributions would be identical if there were no correlations between the momenta of the two neutrons. There is clearly a suppression of recoil events at small momenta (dashed curve), whereas the distribution for the relative motion of the two neutrons (solid curve) has a maximum at small momenta. We study the different components of the recoil momentum distributions in more detail in the next section.

The calculated decay-energy spectrum is shown in Fig. 3 together with the data [2]. The measured spectrum is seen to be shifted towards higher excitations when compared to the model prediction. We saw a similar shift in the recoil momentum distribution, shown Fig. 1(a). In fact, the discrepancies in the two figures may be related. To illustrate this point, we recall the expressions that were used in the data analysis to determine the decay en-
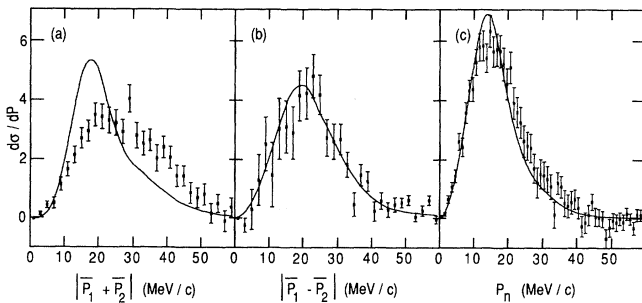

FIG. 2. Three-dimensional momentum distributions, Eq. (7), for the ^{9}Li recoil (dashed curve) and the relative motion of the two neutrons (solid curve) in the rest frame of the ^{11}Li$\rightarrow^9$Li$+n+n$ breakup reaction on a lead target at 28 MeV/nucleon.

ergy and the ^{9}Li recoil momentum, Eq. (13) of Ref. [2],

$$E_{\text{dec}} = \tfrac{1}{4}m(\mathbf{v}_1 - \mathbf{v}_2)^2 + \tfrac{9}{11}m\mathbf{v}_{9,2n}^2 \ , \qquad (8)$$

$$\mathbf{P}_9 = \tfrac{18}{11}m\mathbf{v}_{9,2n} \ , \qquad (9)$$

where $\mathbf{v}_1$ and $\mathbf{v}_2$ are the velocities of the two neutrons and $\mathbf{v}_{9,2n}$ is the relative velocity of the fragment and the two-neutron system. The data shown in Figs. 1 and 3 were corrected for the average shift, $\langle \mathbf{v}_{9,2n} \rangle$, observed in the original measurement (see Fig. 14 of Ref. [2]), which was ascribed to the post-acceleration effect. There may also be fluctuations in this velocity, caused by the same mechanisms that generated the average velocity shift, namely the post-acceleration effect, energy loss in the target, or whatever may change the velocity of the fragment on its way to detection. This will cause fluctuations in the de-

FIG. 1. Momentum distributions for (a) the ^{9}Li recoil, (b) the relative motion of the two neutrons, and (c) for single neutrons in the rest frame of the ^{11}Li$\rightarrow^9$Li$+n+n$ breakup reaction on a lead target at 28 MeV/nucleon. The data are from Ref. [2]. The calculated curves (normalized to 100) include the detection efficiency.
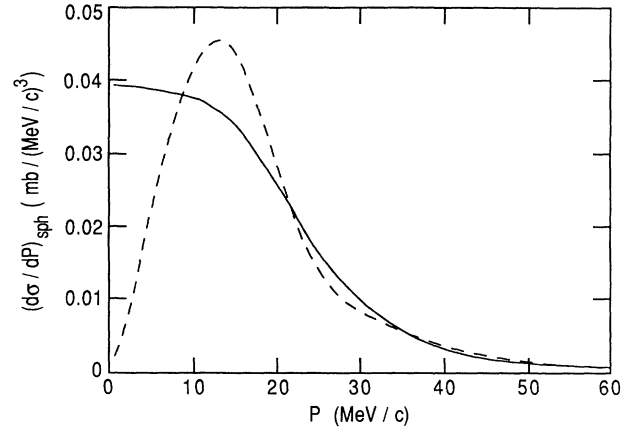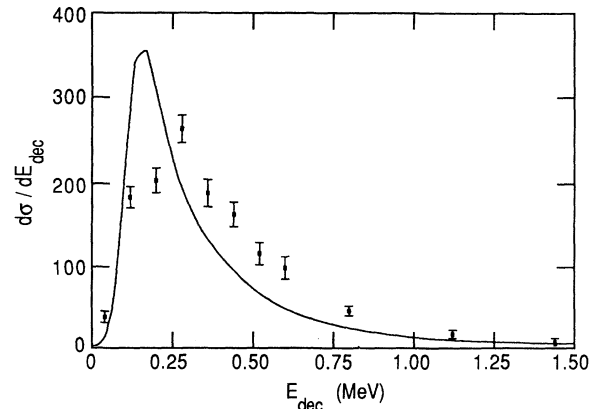

FIG. 3. Decay-energy spectrum for (^{11}Li,^{9}Li) reactions on a lead target at 28 MeV/nucleon. The data points are from Ref. [2]. The calculated curve (normalized to 100) includes the detection efficiency.

cay energy and in the recoil momentum, and from Eqs. (8) and (9) we obtain the following relation,

$$\langle \delta E_{\text{dec}} \rangle = \frac{9}{11} m \langle (\delta v_{9,2n})^2 \rangle = \frac{11}{36} \frac{1}{m} \langle (\delta P_9)^2 \rangle . \quad (10)$$

If the fluctuations in velocity are of the same order of magnitude as the observed shift, of $0.009c$, one obtains from Eq. (10) a fluctuation in the decay energy of 0.076 MeV and one in the recoil momentum of 14 MeV/c. This is the order of magnitude that is needed to explain the discrepancies between the data and our calculations. A more detailed study and modeling of these fluctuations is clearly needed.

The Coulomb dissociation cross section that we obtain is $\sigma_C = 4.5$ b at 28 MeV/nucleon on a lead target. We expect the nuclear part of the (^{11}Li, ^{9}Li) cross section to be of the order of $\sigma_{\text{nuc}} = 1 \pm 0.3$ b, based on the independent-particle-model calculations performed by Sustich [18]. He also assumed a two-neutron separation energy of 0.2 MeV, but spatial correlations between the valence neutrons may reduce his estimate slightly, Ref. [11]. Our estimated total cross section is 5.5 b, which is slightly higher than the value, 5.1 ± 0.3 b, obtained from the telescope data [2]. The neutron-coincidence data were obtained by subtracting a background from crosstalk events and from breakup events that occurred in the detectors. The resulting spectrum appears to be insensitive to events with large excitation energies, say larger than 1.5 MeV (see Ref. [2]). The Coulomb dissociation cross section that we obtain for this cutoff is $\hat{\sigma}_C = 3.9$ b, which can be compared to the measured cross section of 3.6 ± 0.4 b obtained from the two-neutron coincidence data. The measured single-neutron cross section is 8.3 ± 0.5 b. This can be compared to our estimate of $2\hat{\sigma}_C + \sigma_{\text{nuc}} = 8.8$ b, assuming multiplicities of 2 and 1 for Coulomb- and nuclear-induced reactions, respectively. All of these estimated cross sections are consistent with the measurements. They are all at the upper edge of the experimental uncertainty; this may be related to the fact that the experimental binding energy [13] is somewhat larger than our model prediction.

B. Momentum distributions for the ^{9}Li recoil

It may be difficult to study the detailed energy and angular correlation between the two emitted neutrons directly from the three-body coincidence measurements because of limited statistics. It is therefore useful to consider other observables that may contain some information, for example, about the angular correlation. In this section we discuss the different components of the momentum distribution for the ^{9}Li fragment. We define the longitudinal distribution by,

$$\frac{d\sigma}{dP_L} = \int d\mathbf{k}_1 d\mathbf{k}_2 \frac{d^6\sigma}{d\mathbf{k}_1 d\mathbf{k}_2} \delta(P_L + k_{1z} + k_{2z}) , \quad (11)$$

where the z axis points in the beam direction. We show in Fig. 4 the calculated longitudinal momentum distribution at 66 MeV/nucleon on a tantalum target, together with the data obtained by Orr *et al.* [7]. The distribution is actually slightly narrower than the distribution that we
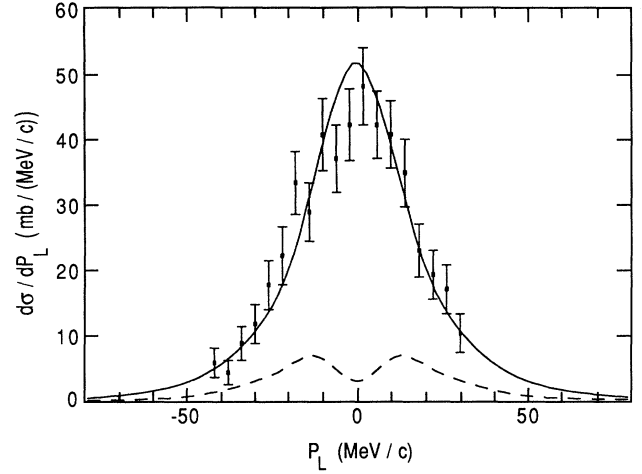

FIG. 4. Longitudinal momentum distribution for the ^{9}Li fragment in (^{11}Li,^{9}Li) reactions on a tantalum target at 66 MeV/nucleon. The solid curve has been calculated from Eq. (11). The dashed curve is the separate contribution from longitudinal dipole excitations. The data are from Ref. [7].

obtained in Ref. [10], where we neglected the angular correlation between the two emitted neutrons. The measured distribution is slightly broader than that in our new calculation. This may be caused by the post-acceleration effect discussed in the preceding section.

Upon inserting Eq. (2) into Eq. (11), we see that the longitudinal momentum distribution is the sum of two contributions: one due to longitudinal dipole excitations; the other to transverse dipole excitations. It is convenient to express this momentum distribution in terms of the transverse dipole-strength distribution alone, since transverse dipole excitations dominate the cross section. We can achieve this by using the facts that the two dipole-strength distributions are invariant under rotations around their respective symmetry axes, and that they are related by a simple rotation of 90°, say, around the y axis. Thus we obtain the expression

$$\frac{d\sigma}{dP_L} = \int d\mathbf{k}_1 d\mathbf{k}_2 \frac{d^6 B^T(E1)}{d\mathbf{k}_1 d\mathbf{k}_2} [g_L(\xi)\delta(P_L + k_{1x} + k_{2x})$$
$$+ g_T(\xi)\delta(P_L + k_{1z} + k_{2z})] , \quad (12)$$

where the z axis is along the beam direction and the x axis is the symmetry axis for the transverse dipole-strength distribution defined earlier. The two contributions are quite different, as illustrated by the dashed curve in Fig. 4, which shows the separate contribution from longitudinal excitations. However, it would be difficult to observe the different character of the two distributions, since transverse excitations dominate the total dipole cross section at intermediate energies (78% at 28 MeV/nucleon and 95% at 800 MeV/nucleon).

The energy dependence is illustrated in Fig. 5, where we show the longitudinal momentum distribution at 28 MeV/nucleon (solid curve) and at 800 MeV/nucleon

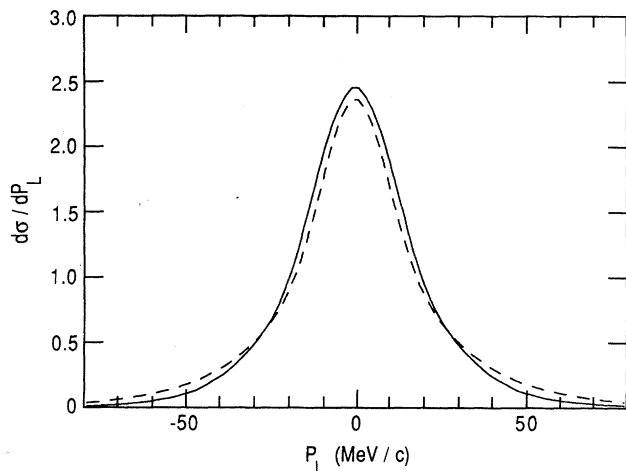FIG. 5. Calculated longitudinal momentum distributions for the ^{9}Li fragment in (^{11}Li,^{9}Li) reactions on a lead target at 28 MeV/nucleon (solid curve) and 800 MeV/nucleon (dashed curve). The two distributions have been normalized to 100.

(dashed curve), both for a lead target. The half-width (at half maximum) has decreased slightly at the higher beam energy, from 17 to 16 MeV/c, whereas the tail of the distribution has become larger. In fact, the total spread has increased from 21 to 26 MeV/c. The reduction in the width for increasing beam energy is due to angular correlations. Thus, if we ignore the angular correlation, the half-width of the distribution increases from 20 to 22 MeV/c, going from 28 to 800 MeV/nucleon. In either case, the energy dependence of the width is weak, and it will be interesting to see what future measurements will show.

Let us finally take a look at the transverse momentum distribution for the ^{9}Li recoil. We can, in fact, distinguish between two such distributions, an in-plane and an out-of-plane distribution, where the plane in question is the scattering plane of the incident projectile and the target nucleus. Similar to the derivation of Eq. (12), we obtain the following expressions:

$$\frac{d\sigma}{dP_{T,\text{in}}} = \int d\mathbf{k}_1 d\mathbf{k}_2 \frac{d^6 B^T(E1)}{d\mathbf{k}_1 d\mathbf{k}_2}$$

$$\times [g_L(\xi)\delta(P_{T,\text{in}}+k_{1z}+k_{2z})$$

$$+g_T(\xi)\delta(P_{T,\text{in}}+k_{1x}+k_{2x})] , \qquad (13)$$

for the in-plane distribution, and

$$\frac{d\sigma}{dP_{T,\text{out}}} = \int d\mathbf{k}_1 d\mathbf{k}_2 \frac{d^6 B^T(E1)}{d\mathbf{k}_1 d\mathbf{k}_2}[g_L(\xi)+g_T(\xi)]$$

$$\times\delta(P_{T,\text{out}}+k_{1z}+k_{2z}) , \qquad (14)$$

for the out-of-plane distribution. The two distributions we obtain at 28 MeV/nucleon for a lead target are shown in Fig. 6. Here the in-plane distribution (solid curve) shows a characteristic dip for a vanishing momentum transfer in that direction. The dip is, of course, related to the minimum we saw in Fig. 2 for the spherical part of the three-dimensional recoil momentum distribution.
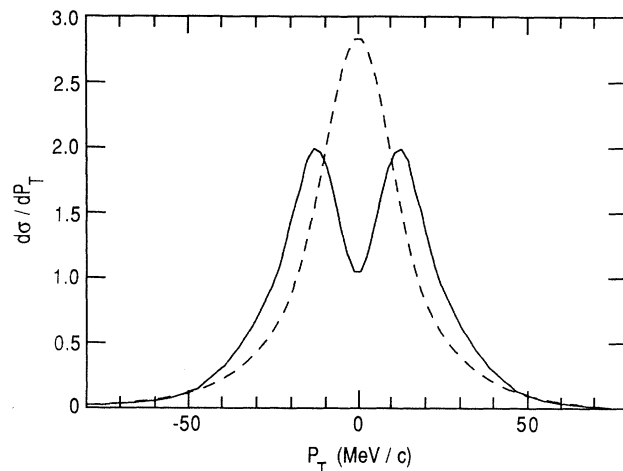
FIG. 6. Calculated transverse momentum distributions for the ^{9}Li fragment in (^{11}Li,^{9}Li) reactions on a lead target at 28 MeV/nucleon. The solid curve is the in-plane distribution defined in Eq. (13) and the dashed curve is the out-of-plane distribution defined in Eq. (14). The two distributions (both normalized to 100) do not include the effect of Coulomb deflection.

The minimum remains visible when integrated over the longitudinal and transverse out-of-plane components.

The out-of-plane distribution (14), obtained by integrating over the longitudinal and transverse in-plane components, is illustrated by the dashed curve in Fig. 6. It is almost identical to the longitudinal momentum distribution shown in Fig. 5. This follows directly from Eqs. (12) and (14) since transverse dipole excitations dominate the cross section (i.e., $g_T \gg g_L$). The two distributions are mainly determined by the momentum component $-(k_{1z}+k_{2z})$, which is perpendicular to the symmetry axis for transverse dipole excitations. The transverse in-plane distribution, Eq. (13), is mainly determined by the momentum component $-(k_{1x}+k_{2x})$, which is parallel to the transverse symmetry axis.

The fact that the longitudinal and transverse out-of-plane distributions both have a maximum at zero, whereas the transverse in-plane distribution has a minimum at zero, is consistent with the angular correlation discussed in Ref. [10]. There we found that the most probable emission of the two neutrons appears when the two neutrons are emitted on opposite sides of the symmetry axis with an opening angle close to 90°. For this configuration one finds that the component of the ^{9}Li recoil momentum, which is along the symmetry axis, is generally larger than the two perpendicular components. It is therefore not surprising that the transverse in-plane distribution shown in Fig. 6 is suppressed at zero.

The transverse momentum distributions we have calculated may differ significantly from measured distributions. One complication is the overall Coulomb deflection of the projectile and the fragment. This can have a strong effect on the transverse distributions, whereas the longitudinal momentum distribution is much less sensitive to this effect. In addition, it may be difficult in an actual measurement to separate the two transverse distributions we have discussed.

IV. CONCLUSION

Perturbation theory and the three-body Hamiltonian model give a rather good description of the various momentum distribution and correlation functions measured in the (^{11}Li, ^{9}Li$+n+n$) breakup reaction, except for the ^{9}Li recoil momentum distribution and the decay-energy spectrum. We have also presented predictions of additional observables that can be measured and that may give some information about the angular correlation between the two emitted neutrons. The disagreement for the recoil momentum distribution and the decay-energy spectrum may be related to Coulomb acceleration effects, which can only be treated in a higher-order reaction theory.

[1] K. Ieki et al., Phys. Rev. Lett. 70, 730 (1993).
[2] D. Sackett et al., Phys. Rev. C 48, 118 (1993), this issue.
[3] S. Shimoura et al. (unpublished).
[4] T. Kobayashi et al., Phys. Lett. B 232, 51 (1989).
[5] R. Anne et al., Phys. Lett. B 250, 19 (1990).
[6] T. Kobayashi (unpublished).
[7] N. A. Orr et al., Phys. Rev. Lett. 69, 2050 (1992).
[8] T. Kobayashi et al., Phys. Lett. B 60, 2599 (1988).
[9] G. F. Bertsch and H. Esbensen, Ann. Phys. (N.Y.) 209, 372 (1991).
[10] H. Esbensen and G. F. Bertsch, Nucl. Phys. A542, 310 (1992).
[11] H. Esbensen and G. F. Bertsch, Phys. Rev. C 46, 1552 (1992).
[12] H. Esbensen, in Proceedings of International Symposium on Structure and Reactions of Unstable Nuclei, Niigata, Japan, 1991, edited by K. Ikeda and Y. Suzuki (World Scientific, Singapore, 1992), pp. 178–186.
[13] T. Kobayashi, Nucl. Phys. A 538, 343c (1992).
[14] H. G. Bohlen et al., Z. Phys. A 344, 381 (1993).
[15] W. Benenson (private communication).
[16] J. M. Bang and I. J. Thompson, Phys. Lett. B 279, 201 (1992).
[17] J. M. Bang, L. S. Ferreira, and E. Maglione, Europhys. Lett. 18, 679 (1992).
[18] A. Sustich, Z. Phys. A 342, 31 (1992).